Published in final edited form as:
Nat Struct Mol Biol. 2013 July ; 20(7): 859–867. doi:10.1038/nsmb.2597.

A ternary AppA–PpsR–DNA complex mediates light-regulation of photosynthesis-related gene expression

Andreas Winkler[1], **Udo Heintz**[1], **Robert Lindner**[1], **Jochen Reinstein**[1], **Robert L. Shoeman**[1], and **Ilme Schlichting**[1]

[1]Department of Biomolecular Mechanisms, Max Planck Institute for Medical Research, Heidelberg, Germany.

Abstract

The anoxygenic phototrophic bacterium *Rhodobacter sphaeroides* uses different energy sources depending on environmental conditions including aerobic respiration or, in the absence of oxygen, photosynthesis. Photosynthetic genes are repressed at high oxygen tension, but at intermediate levels their partial expression prepares the organism for using light energy. Illumination, however, enhances repression under semi-aerobic conditions. Here, we describe molecular details of two proteins involved in oxygen- and light-control of photosynthesis gene expression, the light-sensing anti-repressor AppA and the transcriptional repressor PpsR. We combine information from crystal structures of both proteins and their complex with hydrogen-deuterium exchange data to show that light-activation of AppA–$PpsR_2$ affects the PpsR effector region within the complex. DNA-binding studies demonstrate the formation of a light-sensitive ternary AppA–PpsR–DNA complex. Implications of these results for light- and oxygen-regulation are discussed, highlighting new insights into blue-light-mediated signal transduction.

Organisms from all kingdoms of life are able to perceive environmental stimuli required for adaptation to their habitats. The facultatively phototrophic alphaproteobacterium *Rhodobacter sphaeroides* is remarkably versatile in adjusting its energy generation to environmental cues. Aerobic respiration is the preferred mode of deriving energy. A decrease in oxygen tension activates expression of genes that encode components of the photosynthetic apparatus. This prepares the organism for using photosynthesis as an alternative energy source upon oxygen depletion. At intermediate oxygen levels, however, when photosynthesis genes are partially expressed in the dark, light inhibits the formation of the photosynthetic apparatus because the combination of oxygen and photosynthesis results in photo-oxidative stress[1]. Light and oxygen are perceived and integrated by the AppA–PpsR regulatory system, where PpsR is a master repressor of photosynthesis genes and AppA a light and oxygen sensitive anti-repressor[2-7] that can form a non-covalent AppA–$PpsR_2$ complex[4].

AppA senses blue-light via its N-terminal sensor of blue-light using FAD (BLUF) domain[4,5,8] and oxygen via its SCHIC (sensor containing heme instead of cobalamin)

Correspondence should be addressed to A.W. (Andreas.Winkler@mpimf-heidelberg.mpg.de).

Author contributions A.W. and I.S. designed the project. A.W., U.H. and R.L. cloned, expressed and purified AppA variants. U.H. cloned, expressed and purified the PpsR constructs. A.W., U.H. and J.R. performed and interpreted photocycle, MST and MALS experiments. A.W. carried out EMSAs as well as HDX-MS. A.W. crystallized the AppA variants and solved their structure. U.H. crystallized PpsR and the AppA–$PpsR_2$ core-complex and A.W. and U.H. determined the corresponding structures. A.W., R.L., J.R. and R.S. analyzed and interpreted HDX data. A.W. and I.S. wrote the manuscript. All authors discussed the results and the manuscript.

Accession codes Coordinates and structure factors have been deposited in the Protein Data Bank, with accession codes 4HH0 for $AppA_{\Delta C}$, 4HH1 for wild-type AppA Δ399, 4HH2 for PpsR ΔHTH and 4HH3 for the AppA–$PpsR_2$ core complex.

Europe PMC Funders Author Manuscripts

domain that also mediates the AppA–$PpsR_2$ interaction[6,7]. The cysteine-rich C-terminus of AppA is dispensable for oxygen-sensing[7]. The multi-domain protein[9] PpsR consists of three PAS domains (designated N-domain[10,11], PAS1 and PAS2), a glutamine-rich region (Q-linker) and a helix-turn-helix (HTH) motif (Fig. 1**a**) for binding to palindromic DNA (TGTc-N_{10}-gACA)[12]. A redox-sensitive cysteine residue in the HTH domain[13] was reported to form an intramolecular disulfide bond[4]. In addition, PpsR can interact with heme[14].

The basis of light-dependent signaling by AppA–PpsR has remained unclear. Biochemical data suggest the formation of an AppA–$PpsR_2$ complex in the dark that dissociates upon illumination[4]. Molecular details of such a mechanism are, however, unknown and crystal[15,16] and solution[17] structures have only been determined of the isolated BLUF domain, providing limited mechanistic insights to light-induced conformational changes[18,19]. Therefore, we set out to obtain structural insights into the light-dependence of AppA–$PpsR_2$ interactions and their consequences on DNA-binding. Here, we present crystal structures of AppA, PpsR and an AppA–$PpsR_2$ core complex. Based on functional studies and structural analysis of light-induced changes using Hydrogen-Deuterium exchange coupled to mass spectrometry (HDX-MS), we propose a direct light-signaling mechanism via a ternary AppA–PpsR–DNA complex. We show that AppA–$PpsR_2$ stability is only mildly affected by blue-light. Rather, this complex interacts with PpsR-binding sites on DNA preventing formation of the PpsR-DNA repressor complex in a light-dependent manner. Together, these results highlight details of the molecular mechanism and provide a new model of light-modulated regulation of photosynthesis genes in *R. sphaeroides*.

Results

Characterization of AppA, PpsR and their complex

To understand how blue-light sensing in AppA affects DNA-binding of PpsR, we generated protein constructs encompassing the domains required for protein complex formation and light-signal transduction (Fig. 1**a**). We addressed the oligomeric state of full-length PpsR, which is described as either a dimer[11] or tetramer[9], by multi-angle light-scattering (MALS) analysis coupled to size exclusion chromatography. Quantification of the average molar mass yielded ~150 kDa (Fig. 1**b**), suggesting a trimer based on 51 kDa per monomer. However, pronounced peak tailing and a continuous decrease of the molar mass signal (Fig. 1**b**) suggested a dynamic equilibrium of PpsR tetramers and dimers. We quantified this transition using microscale thermophoresis (MST, Supplementary Note) and obtained a K_d of 0.9 μM for the 2 $PpsR_2 \leftrightarrows PpsR_4$ equilibrium based on $PpsR_2$ concentration (Fig. 1**b** inset). If not indicated otherwise, the AppA construct used throughout this study was AppA Δ399 C20S (see Supplementary Note and Supplementary Figure 1**a**,**b**,**c**,**d**), which is subsequently referred to as $AppA_{\Delta C}$. We quantified the $AppA_{\Delta C}$ interaction with dimeric PpsR (AppA–$PpsR_2$ stoichiometry[4]) using MST and determined a K_d of 1.3 μM for $AppA_{\Delta C}$–$PpsR_2$ (Fig. 1**c**).

Interestingly, the higher kinetic stability of $AppA_{\Delta C}$–$PpsR_2$ (Supplementary Fig. 1**c**) compared to $PpsR_4$ (Fig. 1**b**) observed upon gel filtration suggests that also association and dissociation kinetics influence the available concentration of molecular species thereby affecting light-sensing and DNA-binding.

Illumination of $AppA_{\Delta C}$–$PpsR_2$

Unexpectedly, we observed no light-induced dissociation of $AppA_{\Delta C}$–$PpsR_2$, as described previously[4], when performing gel filtration experiments with continuous illumination at $AppA_{\Delta C}$ concentrations above the K_d. Illumination rather induced changes in elution volumes for $AppA_{\Delta C}$ and $AppA_{\Delta C}$–$PpsR_2$, indicating conformational changes of both

species (Supplementary Fig. 2**a**). To circumvent the problem of limited light penetration into the column, we performed native polyacrylamide gel electrophoresis (PAGE) under dark and light conditions (Supplementary Fig. 2**b**,**c**). These experiments confirmed the light stability of the binary complex and we observed a retardation of $AppA_{\Delta C}$–$PpsR_2$ migration similar to the size exclusion experiments (Supplementary Fig. 2**a**). Semi-quantitative evaluation of the $AppA_{\Delta C}$–$PpsR_2$ affinity (Fig. 2**a**) showed that complex stability is only mildly affected by illumination. The effective concentration for 50% response (EC_{50}) increases only 1.6-fold from dark (1.4 μM) to light (2.3 μM). Additional experiments performed with an AppA variant (Q63E) locked in the light state further confirmed that light-activated AppA interacts with PpsR (Supplementary Fig. 2**d**,**e**).

AppA modulates DNA-binding of PpsR in a ternary complex

Since light-activation of AppA affects PpsR-mediated transcriptional regulation, we characterized the influence of AppA on PpsR-DNA interaction. Using electrophoretic mobility shift assays (EMSAs, Supplementary Fig. 3**a**) we measured PpsR-binding to a 70 base pair (bp) (named *puc I*) or 250 bp (*puc II*) DNA fragment, both containing the two palindromes of the *R. sphaeroides puc* promoter and differing only in their extensions. Semi-quantitative data evaluation showed the characteristic cooperative binding (Fig. 2**b**) described previously[4,6]. Using the Hill equation we obtained an EC_{50} of 1 μM and a Hill-coefficient of 4.3 ± 0.3 for DNA-binding, which corresponds to the theoretical maximum for the four binding sites present in two *puc* palindromes. Four HTH motifs provided by a PpsR tetramer are theoretically sufficient to interact with all four binding sites; however, an active-site titration of PpsR with DNA (Fig. 2**b** inset and Supplementary Fig. 3**b**) indicated that eight PpsR molecules are required for saturation of *puc II.*

To characterize the influence of AppA on DNA-binding properties of PpsR, we tested different concentrations of $AppA_{\Delta C}$. Below 1 μM the apparent affinity of PpsR for *puc I* was slightly reduced compared to PpsR alone (Supplementary Fig. 3**c**), as reported previously[4,6]. Interestingly, we noted an additional faint band and increasing the $AppA_{\Delta C}$ concentration to 1.5 μM resulted in an increase of intensity of this newly observed species, indicating the formation of a ternary $AppA_{\Delta C}$–PpsR–*puc I* complex (Fig. 2**c** and Supplementary Fig. 3**d**). Importantly, even an excess of PpsR was not able to compete with $AppA_{\Delta C}$–$PpsR_2$ for DNA, suggesting a higher affinity or higher kinetic stability of the ternary complex. A comparison of the transitions from free to bound DNA (~0.5–1.5 μM vs. ~0.25–2.5 μM PpsR for $PpsR_8$ vs. $AppA_{\Delta C}$–$PpsR_2$, respectively, Supplementary Fig. 3**a** vs. Fig. 2**c**) demonstrates that the ternary complex is formed at lower PpsR concentrations compared to $PpsR_8$ and that $AppA_{\Delta C}$–$PpsR_2$-binding to DNA shows reduced cooperativity.

Illumination reduces the affinity of $AppA_{\Delta C}$–$PpsR_2$ for DNA

While previous studies propose light-induced AppA–$PpsR_2$ dissociation[4], our new results of its light-response and the observation of an AppA–$PpsR_2$–*puc* complex warrant analysis of the light-influence on this ternary system. To that end, we compared EMSAs performed with varying concentrations of the individual components under dark (Fig. 2**c**) and light conditions (Fig. 2**d**).

At 1.5 μM $AppA_{\Delta C}$ and increasing concentrations of PpsR the fraction of PpsR-bound DNA increased upon illumination (Fig. 2**d**) due to the light-dependent dissociation of $AppA_{\Delta C}$–$PpsR_2$ (Supplementary Fig. 3**e**), as suggested previously[4]. However, similar experiments with higher $AppA_{\Delta C}$ concentrations (5 μM $AppA_{\Delta C}$, 3 μM PpsR – to form the binary complex irrespective of light) demonstrated that illumination reduces the affinity of $AppA_{\Delta C}$–$PpsR_2$ for DNA (Fig. 2**e** and Supplementary Fig. 3**f**). This is indicated by the disappearance of the ternary complex and a smear towards free DNA, which is then

available to uncomplexed PpsR (5 μM $AppA_{\Delta C}$, 13 μM PpsR) for binding (Fig. 2**e** lane 3). This again highlights the importance of the kinetic stability of different species involved in the light response.

A detailed analysis of ternary complex illumination at $AppA_{\Delta C}$ concentrations (20 μM) enabling formation of $AppA_{\Delta C}$–$PpsR_2$ throughout the PpsR titration range (0–30 μM, Fig. 2**f**), showed that stable ternary complex formation occurs only at one order of magnitude higher PpsR concentrations compared to dark conditions (Fig. 2**c**). However, a quantitative comparison is complicated because the cooperativity of DNA-binding and the kinetics of ternary complex disassembly are affected by illumination.

The $AppA_{\Delta C}$ structure supports the dual sensor model

To identify elements affected by illumination, we solved the crystal structure of $AppA_{\Delta C}$ to 2.6 Å resolution (Table 1), revealing molecular details beyond the BLUF domain. A schematic and cartoon representation of the overall structure is shown in Figure 3**a**,**b** and Supplementary Figure 4. The core BLUF domain closely resembles the structure of the isolated domain (root mean square deviation (RMSD) 0.3 Å to AppA BLUF 1–124[16]), in particular, strand $\beta5_{B\_A}$ (subscripts denote the domain and the protein with BLUF, 4HB and SCHIC for AppA and N, PAS1 and PAS2 for PpsR) displays a kink corresponding to the Trp_{out} conformation[16]. Interestingly, Trp104 is sandwiched between the core β-sheet of the BLUF domain and an amphipathic helix (amino acid (aa) 141–162) capping this β-sheet (Fig. 3**c**). To exclude that the C20S substitution causes the Trp_{out} orientation, we solved the AppA Δ399 wild-type structure (pdb 4HH1) showing an identical Trp104 conformation. The linker between the BLUF and SCHIC domains consists of the BLUF capping helix, some stretches without secondary structure elements, followed by a four helix bundle (4HB). The SCHIC domain has a flavodoxin-like fold as expected from its relationship with the cobalamin-binding superfamily[7]. Structural details of the SCHIC domain are described in the Supplementary Note and Supplementary Figure 4**b**. An interesting feature of the $AppA_{\Delta C}$ structure is the weak interaction between the BLUF and SCHIC domains. A surface representation (Supplementary Fig. 4**c**) suggests that both domains use the linker region and the 4HB as “binding platforms” without strong interactions at the BLUF–SCHIC interface. This is in line with the current view that AppA integrates two stimuli and communicates them to PpsR.

Illumination affects central elements of the BLUF domain

Comparative HDX experiments performed under identical experimental conditions for two states of a protein provide information on their structural differences. Therefore, HDX is ideally suited for complementing crystallographic studies in terms of AppA–$PpsR_2$ complex formation and illumination. In addition, differences in deuterium exchange kinetics correlate with secondary structure stability (Supplementary Note and Fig. 3**d**).

Figure 3**e** shows the overall structure of $AppA_{\Delta C}$ colored according to the observed changes in deuterium uptake between light- and dark-states (ΔD_{rel} represents the absolute difference in relative deuterium incorporation). Shades of red correspond to elements with an increased deuterium uptake in the light-state, representing a destabilization of secondary structure or deprotection due to loss of interaction. Accordingly, blue indicates stabilization upon complex formation or an increase in secondary structure stability. Full details of all comparative experiments are shown in Supplementary Movies 1–6. Interestingly, changes in deuterium uptake at initial time points are restricted to the BLUF domain and the capping helix. A substantial stabilization upon illumination is observed for the $(\alpha1–\beta2)_{B\_A}$ element, including Ser41 and Asn45 interacting with the flavin cofactor, and the $\beta5_{B\_A}$ strand

containing Met106. Importantly, the central part of the capping helix becomes slightly destabilized upon illumination, suggesting an involvement in light-signal integration.

The importance of PAS domains for oligomerization of PpsR

To obtain a better understanding of PpsR, we set out to determine its structure. We crystallized a construct lacking the HTH motif ($PpsR_{\Delta HTH}$, Fig. 4**a**) and determined the structure to 2.8 Å resolution (Table 1). This revealed a tetrameric assembly of the triple PAS protein in the asymmetric unit (Fig. 4**b**), which is composed of two antiparallel dimers each having a parallel dimerization interface ranging from the N-terminal PAS domain (N-domain) via the α-helical Q-linker (αQ) to the PAS1 domain. While the PAS2 domains also form a homodimer, the overall dimer symmetry is broken due to interaction of the PAS2 domains with αQ of the other dimer. Based on the C-termini of the PAS2 domains the position of the HTH motif is expected to be close to αQ of the second dimer (Fig. 4**c** and Supplementary Fig. 5) which might contribute to the strong evolutionary conservation of this region (Supplementary Fig. 6**a**). While structural rearrangements upon DNA-binding cannot be excluded, the distant positioning of two HTH dimers in the tetramer is unlikely to result in efficient binding of *puc* palindromes that are separated by a half-turn of the DNA double-helix. Interestingly, αQ provides another antiparallel oligomerization interface with a symmetry-related tetramer, thereby forming an octameric assembly (Supplementary Fig. 5**a**,**b**). In this case, the proposed location of the HTH motifs would be ideally positioned for DNA-binding (Fig. 4**c**), explaining the cooperativity and the 1:8 stoichiometry of *puc*:PpsR binding, respectively, as derived from our active-site titration.

$AppA_{\Delta C}$–$PpsR_2$ formation affects elements of light-signaling

We addressed structural changes of $AppA_{\Delta C}$–$PpsR_2$ formation and illumination by HDX (Fig. 4**d**,**e**,**f**,**g**). The complex formation induced changes in deuterium exchange mapped onto the structures (Fig. 4**d**,**f**) show a pronounced stabilization of the 4HB and the BLUF capping helix in $AppA_{\Delta C}$. In addition, the N-terminal region of SCHIC, extending from the linker to the 4HB via $(\beta1, \alpha1, \beta2 \text{ to } \alpha2)_{S\_A}$ experiences a reduction in deuterium exchange upon complex formation. Several of these elements show above average deuterium incorporation in free $AppA_{\Delta C}$ (Fig. 3**d**). Interestingly, not only the capping helix but also additional light-responsive BLUF elements show changes upon complex formation. While the $(\alpha1–\beta2)_{B\_A}$ region is destabilized in the presence of PpsR, the $\beta5_{B\_A}$ strand shows a similar stabilization to that observed upon illumination. In addition, the $(\beta1–\alpha1)_{B\_A}$ and $(\beta5–\text{capping helix})_{B\_A}$ loop regions become stabilized upon complex formation.

Deuterium incorporation characteristics of PpsR alone (Supplementary Fig. 6**b**) demonstrated that, similar to AppA, regions involved in complex formation (Fig. 4**f**) belong to elements with above average deuterium incorporation. This is most pronounced for parts of the Q-linker region that exhibit bimodal deuterium incorporation characteristics (EX1 kinetics[20]) reflecting complex dissociation during labeling (Supplementary Fig. 6**c**). This extreme form of deuterium exchange is caused by a faster chemical exchange rate of free PpsR compared to the re-association kinetics of the protected $AppA_{\Delta C}$–$PpsR_2$ species. This is supported by HDX experiments performed with different AppA concentrations (Supplementary Fig. 6**d,e,f**). Analysis of the titration curve using the law of mass action provided a K_d estimate of ~1.5 μM, in agreement with our MST data. Additional elements with pronounced stabilization are observed in the N-domain including loops around $\alpha1_{N\_P}$ and $\alpha3_{N\_P}$. Similarly, $\beta4_{1\_P}$ and $\beta5_{1\_P}$ and their connecting loop become stabilized upon complex formation. Interestingly, the PAS2 domain behaves opposite and complex formation leads to destabilization of the $\alpha3_{2\_P}$, $\beta4_{2\_P}$ and $\beta5_{2\_P}$ elements, which, given the AppA–$PpsR_2$ stoichiometry, supports a role of this region in PpsR homo-tetramerization as seen in the crystal structure (Fig. 4**b**). In addition, this suggests an interaction interface of

Europe PMC Funders Author Manuscripts

AppA on αQ preventing PpsR oligomerization by blocking the PAS2-binding site. The HTH region (Fig. 5**a**-**e**) shows only sub-threshold stabilization upon complex formation, which indicates that $AppA_{\Delta C}$ does not prevent DNA-binding of PpsR by interacting with the HTH motif.

HDX measurements of light-adapted $AppA_{\Delta C}$–$PpsR_2$ additionally support that illumination does not lead to complex dissociation (Fig. 4**e**,**g**), due to sustained stabilization of αQ and the N- and PAS1-elements described above. The light-red color of a part of αQ corresponds to only ~10 % of the stabilization upon complex formation and can be explained with a small, light-induced reduction in AppA–$PpsR_2$ concentration due to experimental conditions limiting light-independent saturation of the binary system (cf. Fig. 2**a**). Therefore, the N–Q–PAS1 domains of PpsR form a light-independent core binding interface with AppA. The PAS2 domain, on the other hand, shows partial reversibility of changes observed upon complex formation. Most importantly, the C-terminal HTH motif is pronouncedly stabilized, showing EX1-like kinetics for peptides from this region (Fig. 5**b**). This might originate either from a light-state AppA-induced HTH dimerization or interaction with light-responsive AppA elements.

HDX changes induced by illumination of PpsR-complexed $AppA_{\Delta C}$ are clustered around the BLUF domain and partially correspond to observations of isolated $AppA_{\Delta C}$. Substantial stabilization is observed in the $(\alpha1–\beta2)_{B\_A}$ region while the central part of the capping helix partially reverts to a more flexible state (Fig. 5**f**-**j**). Apart from these changes only the region between the pairs of helices in the 4HB (aa 213–222) is destabilized. The remaining elements in the 4HB and the SCHIC domain are unaffected by illumination and therefore belong to the core interface defined for PpsR above. Importantly, the observation of light-responsive elements from the BLUF core via the capping helix to PAS2 and the DNA-binding HTH motif provides a basis for direct light-regulation in the binary complex.

The complex structure suggests BLUF and PAS2–HTH proximity

Based on core complex regions identified by HDX, we generated corresponding constructs of AppA (4HB–SCHIC) and PpsR (N–Q–PAS1). We crystallized their complex and determined its structure to 1.75 Å resolution (Table 1). The observed assembly matches the AppA–$PpsR_2$ stoichiometry and confirms the binding of AppA to αQ (Fig. 6**a**). Additional interactions of AppA with the N- and PAS1-domains of different PpsR protomers lead to a pronounced rotation of ~70° of the PAS1 domain dimer along the αQ axis and explain the observed asymmetry of the complex. Details of the complex interface agree well with our HDX results (Fig. 6**b**). The pronounced stabilization in the $(\alpha3–\beta3)_{N\_P}$ region can be explained by the observed contact with $(\alpha3–\alpha4)_{H\_A}$. Similarly, αQ interacts with $\alpha4_{H\_A}$ and the linker region to the SCHIC domain including $(\alpha1$ and $\beta2)_{S\_A}$. In addition, $(\beta4_1–\beta5_1)_{1\_P}$ is sandwiched between the connecting loop of the 4HB to the SCHIC domain and $(\alpha1–\beta2–\alpha2)_{S\_A}$. The interactions observed in the core complex fully explain the stabilization of all PpsR elements observed by HDX suggesting that the BLUF domain does not interact extensively with PpsR. Rather, we propose that AppA elements stabilized upon complex formation but not contacting PpsR, i.e. $(\alpha1–\alpha2)_{H\_A}$ and the BLUF capping helix, are stabilized internally. Interestingly, these elements are also in close proximity in the $AppA_{\Delta C}$ crystal structure. Combined with the observation that the arrangement of the 4HB and the SCHIC domain is almost identical in the isolated and complex structures (RMSD = 0.6 Å), it is likely that the $AppA_{\Delta C}$ structure resembles that of AppA stabilized upon PpsR-binding. Figure 6**c** shows a combination of the complex structure with the $PpsR_{\Delta HTH}$ and $AppA_{\Delta C}$ structures. In this model the BLUF domain approaches the PAS2–HTH region of PpsR, which can explain the direct transmission of light-induced changes from the photoreceptor to the PAS2–HTH region as observed by HDX (Supplementary Fig. 7). In

addition, the close positioning of the BLUF domain and the DNA-binding element are likely responsible for the light-induced destabilization of the ternary complex observed in EMSAs.

Discussion

The AppA–PpsR system serves as a master regulator of *R. sphaeroides* photosynthesis genes in response to oxygen and light. Our studies on AppA, PpsR and their cognate DNA provide detailed functional and structural insights for both proteins and their complexes with implications for their biological function. The crystal structure of the transcriptional repressor PpsR reveals an intricate tetrameric assembly composed of two head-to-tail PpsR dimers. Both the N- and the PAS1-domains form homodimers between which αQ forms a coiled-coil like structure that serves as binding-site for either PAS2 domains of another PpsR dimer, leading to tetramer formation, or the AppA light-sensor, resulting in an AppA–$PpsR_2$ complex[4]. The relevance of the PpsR tetramer is supported by the evolutionary conservation of the $\alpha 3_{2\_P}$ and αQ interaction. However, the tetramer architecture cannot explain the highly cooperative DNA-binding mode observed for PpsR, because of the large distance between HTH-dimers. In addition, active site titration data support an octameric PpsR species for DNA-binding. Such an assembly is mediated by αQ of symmetry related tetramers and brings two HTH dimers in close proximity allowing them to cooperatively bind to target promoter sequences. The DNA-binding of PpsR octamers was also proposed for homologs from *Bradyrhizobium*[21]. The importance of these oligomeric states is further supported by the requirement of the N-domain for DNA-binding of PpsR *in vivo*[9] and *in vitro*[11]. Based on the PpsR structure this can be rationalized by impaired dimer and tetramer formation of constructs lacking the N-domain, as suggested previously[11], consequently also affecting octamer formation.

In *R. sphaeroides* the action of PpsR is modulated by the anti-repressor AppA. The two proteins form a complex *in vitro* and *in vivo*[3,4], enabling light- and oxygen-dependent regulation of gene expression. Previously, it was suggested that photon absorption by the AppA BLUF domain triggers dissociation of AppA–$PpsR_2$[4]. This model is based on gel filtration data where AppA, PpsR and their complex are observed in comparable quantities, which indicates experimental conditions close to the K_d of the complex. In this case, even subtle changes in affinity will lead to pronounced differences in the relative amounts of involved species. This interpretation is supported by the reduced, but not eliminated, fraction of complex upon illumination[4]. Analogous experiments using AppA concentrations above the K_d of AppA–$PpsR_2$ resulted in no dissociation; moreover, native PAGE and HDX data also do not support substantial light-induced dissociation of the complex. Rather, our data indicate a small light-dependent decrease of AppA–$PpsR_2$ affinity. We identified a light-independent core binding interface, consisting of the 4HB and the SCHIC domain of AppA and the N–Q–PAS1 region of PpsR by combining structural and HDX data. Illumination rather influences the BLUF domain and capping helix of AppA and the HTH motif of PpsR which argues for a light-signaling pathway via allosteric structural changes. This hypothesis is supported by the fact that the AppA–$PpsR_2$ complex also binds to the PpsR-binding sites on DNA. This indicates structural “preorganization” of AppA and PpsR in their complex promoting ternary complex formation and thereby reflecting a form of configurational cooperativity[22]. In contrast to the original binary description of PpsR-binding to DNA as a repressor, the introduction of a third component enables different properties of potential DNA-complexes ($PpsR_8$–DNA vs. AppA–$PpsR_2$–DNA) likely reducing the repressive strength and thereby promoting photosynthesis gene expression. Furthermore, light-modulation of AppA–$PpsR_2$–DNA affinity in addition to the subtle light-induced dissociation of AppA–$PpsR_2$ potentially enhances *in vivo* control. In particular, the concentration dependent competition of the ternary complex with DNA-binding of PpsR provides a fine-tunable control system, responding to illumination over a wider range of

Europe PMC Funders Author Manuscripts

protein concentrations. Importantly, AppA and PpsR expression levels are inversely regulated in response to changing oxygen levels[23]. This results from the interplay between the PrrB–A and AppA–PpsR regulatory cascades where PrrA was shown to positively affect AppA expression upon transition from aerobic to anaerobic conditions[23,24]. These oxygen induced changes in concentration may be sufficient to explain *in vivo* regulation in response to changing light and oxygen levels by the ternary system. Since the cellular concentrations of AppA and PpsR are not known, we cannot exclude a regulatory mechanism based on complex dissociation at concentrations close to its K_d under *in vivo* conditions. However, ternary complex formation occurs already at lower concentrations of PpsR and, therefore, increases the potential for transcriptional regulation as described above. In the new model, the light-dependent repressive effect of AppA under semi-aerobic conditions[6,25] is explained by the interference of BLUF elements with the HTH motif of PpsR. This reduces AppA–$PpsR_2$ affinity for DNA and enables excess PpsR to bind to promoter sequences (Fig. 7). This mechanism is consistent with observations under anaerobic conditions where light-induced repression was demonstrated for a strain lacking the PrrB activator[25].

Our study describes the first detailed structural characterization of a BLUF protein in complex with its non-covalent effector. We revealed molecular details of their interaction interface and also provided structural details of the linker region C-terminal of the BLUF domain and its importance for light-regulated modulation of DNA-binding. Our study contributes to a better understanding of the modularity and details of the signaling process of the BLUF photoreceptor family. Previously published crystal structures of the AppA BLUF domain show two different conformations of strand β5 that result in either Trp104[15] or Met106[16] being positioned in the vicinity of the flavin chromophore, which might originate from the use of different protein constructs[26]. These observations resulted in different mechanisms for the photoreaction and spurred a controversy over the dark state structure of AppA and other BLUF proteins (reviewed in [27]). Our $AppA_{\Delta C}$ structure confirmed that the dark state conformation features Met106 close to the flavin cofactor and Trp104 in the “out” conformation[16] where it contacts residues of the newly observed BLUF capping helix, which interacts with residues of β5 and the BLUF core β-sheet. HDX experiments showed that these structural elements are affected by illumination, which is in line with previous NMR experiments[17,19] and theoretical as well as spectroscopic studies[26,28] on the AppA BLUF domain.

Combined with information from other BLUF proteins, common aspects of light-induced changes in the vicinity of the flavin cofactor are emerging that suggest the β-sheet (especially β5) and the C-terminal extensions of BLUFs to be important for signal transduction (reviewed in [27]). Since HDX is not limited by the size of the system we also addressed the structural changes in AppA–$PpsR_2$. This showed that complex formation is a prerequisite for structuring the C-terminal extension of BLUF, which experiences a pronounced destabilization upon illumination. This increased flexibility enables the BLUF domain to interfere with DNA-binding of the complex, which is in line with *in vivo* data demonstrating restoration of light-signaling upon complementation of a system containing BLUF-less AppA with BLUF provided in *trans*[29].

The requirement of a preformed complex for light-signaling is of general interest not only for BLUF proteins but also for other photoreceptor families. So far, one system comprising a BLUF and an effector domain was characterized structurally and functionally; the light-regulated c-di-GMP phosphodiesterase BlrP1[30]. While some elements involved in transmitting the signal to the effector domain are conserved between BlrP1 and AppA, the arrangement of the C-terminal extensions of the BLUF domains differ substantially. BlrP1 represents a BLUF system that is covalently tethered to its effector, however, the majority of BLUF domains signal via non-covalent interaction[8]. One such system, the BLUF protein

PixD and its partner PixE involved in phototaxis control, has been subject of detailed molecular and physiological characterization[31,32]. Common aspects of light-signaling in the family have, so far, not been described and details of the non-covalent interactions are not known for the majority of BLUF proteins. However, knowledge of the complex interface appears to be critical for addressing structural changes and elucidating how the light-signal is transmitted to the effector. The structural characterization of AppA–$PpsR_2$ not only provides new information in this direction but also highlights an important caveat. Crystal structures obtained from isolated domains need to be interpreted with caution, since effector binding regions may be unstructured without interaction partner.

Combining these results with other currently investigated BLUF systems will allow a separation of system-specific aspects of signal transduction from common features involved in BLUF-signaling, which will be important for enabling a rational design of artificial BLUF-based photosensors with application in the growing field of optogenetics[33].

Online methods

Protein expression and purification

We generated AppA constructs by PCR amplification from wild-type pET28_AppA (provided by P. Hegemann). For Ni-NTA based affinity purification, a C-terminal hexa-histidine-tag was included in reverse primers for AppA constructs. Primers for amplifying the full-length, Δ399 and 4HB–SCHIC domain AppA variants are described in Supplementary Table 1. The C20S mutation was introduced in pET21_AppA_full-length and pET28_AppA_Δ399; the Q63E mutation was generated in pET28_AppA_Δ399. In both cases, site-directed mutagenesis was performed according to the QuikChange method (primers in Supplementary Table 1) and correct clones were identified by DNA-sequencing.

An *E. coli* codon optimized gene (GeneArt) served as template for amplification of different PpsR constructs. We generated PCR products representing full-length PpsR, the ΔHTH and the N–Q–PAS1 construct (primers in Supplementary Table 1). The PCR products were cloned into pET_M11 (provided by G. Stier) for using the TEV-cleavable N-terminal histidine-tag during purification.

Protein expression was performed in *E. coli* BL21 (DE3). Cultures were induced with IPTG at an optical density of 0.6–0.9. All constructs except full-length AppA were expressed at 18 °C overnight in the presence of 0.2 or 0.5 mM IPTG for AppA or PpsR, respectively. Full-length AppA was expressed at 24 °C for 6 hours with 0.2 mM IPTG. All AppA experiments from the point of induction onwards were carried out under safe-light conditions, if not stated otherwise. Cells were harvested by centrifugation and the pellets resuspended in buffer A (20 mM CHES pH 9, 10 mM imidazole, 300 mM NaCl and 5 % (weight per volume (w/v)) glycerol) including EDTA-free protease inhibitor (Roche). We performed cell lysis using a microfluidizer (Microfluidics) and clarified lysates by ultracentrifugation at 180,000 g prior to Ni-NTA chromatography. The column was washed with buffer A containing 50 mM imidazole and the protein eluted in buffer A with 200 mM imidazole. AppA fractions incubated with excess FMN were concentrated using Amicon centrifugal filter units and loaded onto a Superdex 200 10/300 GL column equilibrated in buffer B (10 mM CHES pH 9, 150 mM NaCl, 5 % (w/v) glycerol).

After elution from the Ni-NTA column PpsR constructs were dialyzed over night against buffer C (10 mM CHES pH 9, 100 mM NaCl, 2 mM DTE, 2 mM EDTA, 5 % (w/v) glycerol) with parallel TEV-cleavage using a ratio of ~1:25 for TEV:substrate. To remove histidine-tagged TEV and the cleaved histidine-tag, the dialyzed sample was reloaded onto the Ni-NTA column and the flow-through used for further purification. Full-length PpsR

was loaded onto a HiTrap Heparin column (GE Healthcare) and eluted with a NaCl gradient in the buffer system used for dialysis. All proteins were finally purified by size exclusion chromatography in analogy to AppA.

Selenomethionine-substituted proteins were expressed in *E. coli* BL21 (DE3) with modified growth media according to[35] and purified as described above.

Static light scattering

25 μM AppA and PpsR were pre-incubated at 4 °C for 30 minutes and subjected to size exclusion chromatography at RT using a Superdex 200 10/300 GL column (GE Healthcare) equilibrated in buffer B. The chromatography system was connected to an 18-angle light scattering detector (Dawn Heleos, Wyatt Technology) combined with a refractive index detector (Waters). We analyzed data with the ASTRA software (Wyatt Technology), providing estimates for the molar mass of eluting species.

Electrophoretic Mobility Shift Assays

We prepared DNA probes based on PCR amplification of the *R. sphaeroides puc* promoter region. We used two probes: *puc I* (70 bp) encompassing the two palindromes required for PpsR-binding with a 14 and 13 bp extension of the operator sequence at the 5′ and 3′ end, respectively, and *puc II* (250 bp) including 112 bp and 95 bp of the operator sequence, accordingly. DNA probes were purified on Superose 6 (GE Healthcare) size exclusion columns equilibrated in 150 mM ammonium bicarbonate buffer. Buffer exchange to buffer B was performed by sequential steps of ultrafiltration in spin columns (Amicon Ultra-4, 10 kDa cut-off, Millipore).

20 nM DNA probes were incubated in buffer D (10 mM CHES pH 9, 150 mM NaCl, 15 % (w/v) glycerol) with varying amounts of purified PpsR and AppA in a total volume of 5 μL containing 0.5 μg heparin. The mixtures were incubated for 10 min at RT and then separated on 10 % Tris–glycine–EDTA pH 9.0 (TGE) gels for *puc I* or 6 % TGE gels for *puc II* containing samples (allowing resolution of different mass and pI ranges for protein and DNA samples) with 50 mM Tris, 380 mM glycine and 1 mM EDTA at pH 9 as running buffer. Gel runs were performed at 4 °C (except where noted otherwise) under either safe-light conditions or with blue-light illumination from a royal-blue (455 nm) collimated LED lamp (Thorlabs). For the latter purpose, samples were pre-irradiated for 2 min at 600 μW cm^{-2} blue-light in the slot and during electrophoresis (10 V cm^{-1} for 160 min) constant illumination of the gel was kept at 30 μW cm^{-2}. Gels were stained with GelRed (Biotium) for DNA-visualization followed by protein staining using InstantBlue (Biozol). For the active site titration we titrated PpsR (2.5 μM) with 100 to 700 nM *puc II*. The gel run was performed at RT for 70 minutes at 10 V cm^{-1}.

Crystallization and structure elucidation

Crystallization was performed at 20 °C. Trigonal crystals of AppA Δ399 wild-type and C20S were grown in hanging-drop geometry using 15 mg mL^{-1} protein and 0.3 M Tris-Cl pH 7.4, 1.3 M NaCl and 0.3 M $MgCl_2$ as reservoir. Growth of selenomethionine labeled $AppA_{\Delta C}$ included 50 mM DTE in the reservoir. Crystals were harvested after a 2 hour soak in reservoir solution saturated with NaCl and cryo-cooled in liquid nitrogen. Trigonal PpsR ΔHTH crystals were grown in hanging-drop vapor-diffusion setups with 0.1 M Tris–Cl pH 8.5, 1 M ammonium sulfate, 12 % (w/v) glycerol, 6 % (w/v) xylitol and 1 % dioxane as reservoir and protein at 30 mg mL^{-1}. Crystals were harvested after 2 weeks and cryo-cooled after cryoprotection in 50 mM Na-P_i buffer pH 6.8, 12 % (w/v) glycerol and 3 M Na-malonate. Selenomethionine labeled protein was crystallized accordingly.

The complex of PpsR N–Q–PAS1 and the AppA 4HB–SCHIC was crystallized in sitting-drop vapor-diffusion geometry. 0.1 M HEPES pH 7, 64 mM tri-sodium citrate, 10 % (w/v) PEG 5000 monomethyl ether was mixed with the preformed complex at a concentration of 8.3 mg mL^{-1} (1.5:2 stoichiometry of AppA:PpsR). For cryoprotection reservoir solution containing 20 % glycerol was added to the drop. After 1 min incubation crystals were harvested and cryo-cooled in liquid nitrogen.

Diffraction data were acquired at 100 K at beamline X10SA at the SLS (PSI, Villingen, Switzerland). Data were processed using XDS[36]. Phasing and refinement was performed with PHENIX[37]. Refinement included an initial simulated annealing (torsion) step followed by several rounds of maximum likelihood least squares refinement of models modified with Coot[38] employing σ_A-weighted $2mF_o$ - DF_c and F_o - F_c electron density maps. Details of the refinement procedures are presented in the Supplementary Note. Data collection, processing and refinement statistics are summarized in Table 1.

Hydrogen Deuterium Exchange – Mass Spectrometry

We incubated separately purified $AppA_{\Delta C}$ and PpsR at 4 °C for 30 min using a 1.1 fold excess of AppA based on the AppA–$PpsR_2$ stoichiometry. Purification of $AppA_{\Delta C}$–$PpsR_2$ was performed on a Superdex 200 10/300 GL column and the pooled complex fractions were concentrated to 200 μM $AppA_{\Delta C}$–$PpsR_2$. We prepared $AppA_{\Delta C}$ in analogy at a concentration of 200 μM and PpsR samples were set up at a final concentration of 400 μM. We performed deuterium labeling in triplicate after a 90 s pre-incubation at 20 °C followed by 20-fold dilution in D_2O with 10 mM CHES, 150 mM NaCl, 5 % glycer(ol-d3), pD 9.5. For complex measurements this resulted in approximately 75 % of $AppA_{\Delta C}$ bound to PpsR in equilibrium. For blue-light measurements we included parallel illumination from a royal-blue (455 nm) collimated LED lamp (Thorlabs) for the pre-incubation step and during labeling providing a light intensity of 600 μW cm^{-2} at 450 nm. Aliquots of 20 pmol (complex and $AppA_{\Delta C}$) or 40 pmol for PpsR were removed after 15 s, 1, 5 and 20 min and quenched in ice cold 200 mM ammonium formic acid pH 2.6 buffer. We then injected the samples into a cooled HPLC setup (0.5 °C). Deuterated samples were digested on a pepsin column (Applied Biosystems) at 10 °C. Resulting peptides were desalted on a 2 cm C18 guard-column (Discovery Bio C18, Supelco) and separated in the presence of 0.6 % formic acid with a 20 min acetonitrile gradient (15 to 50 %) on a reversed phase column (Discovery Bio Wide Pore C18 10 × 0.1 cm − 3 μm) and injected into a maXis ESI–UHR–TOF (Bruker) for measuring deuterium incorporation. For details of data evaluation see Supplementary Note.

Supplementary Material

Refer to Web version on PubMed Central for supplementary material.

Acknowledgments

We acknowledge K.-A. Seifert for excellent technical support. We thank the Dortmund and Heidelberg team for data collection at beamline X10SA (Swiss Light Source, Villingen, Switzerland). We are grateful to A. Meinhart for help with structural data analysis and EMSAs and C. Roome for IT support. We thank M. Müller and M. Gradl for assistance in mass spectrometry. We are grateful to M. Gomelsky and M. Cryle for stimulating discussions and comments on the manuscript and to P. Hegemann (Humboldt University, Berlin, Germany) for providing the pET28_AppA plasmid. We thank G. Stier (Biochemistry Center, Heidelberg University, Germany) for providing the pET_M11 plasmid and the TEV protease clone. We acknowledge financial support by the European Molecular Biology Organization (EMBO): ALTF 1309–2009 (A.W.), the Austrian Science Fund (FWF): J 3242–B09 (A.W.), the German Research Foundation (DFG): FOR526 (I.S.) and the Max Planck Society.

References

1. Shimada H, Iba K, Takamiya K. Blue-Light Irradiation Reduces the Expression of *puf* and *puc* Operons of *Rhodobacter Sphaeroides* under Semi-Aerobic Conditions. Plant and Cell Physiology. 1992; 33:471–475.
2. Gomelsky M, Kaplan S. Appa, a Novel Gene Encoding a Trans-Acting Factor Involved in the Regulation of Photosynthesis Gene-Expression in *Rhodobacter Sphaeroides* 2.4.1. Journal of Bacteriology. 1995; 177:4609–4618. [PubMed: 7642486]
3. Gomelsky M, Kaplan S. Molecular genetic analysis suggesting interactions between AppA and PpsR in regulation of photosynthesis gene expression in *Rhodobacter sphaeroides* 2.4.1. Journal of Bacteriology. 1997; 179:128–134. [PubMed: 8981989]
4. Masuda S, Bauer CE. AppA is a blue light photoreceptor that antirepresses photosynthesis gene expression in *Rhodobacter sphaeroides*. Cell. 2002; 110:613–623. [PubMed: 12230978]
5. Braatsch S, Gomelsky M, Kuphal S, Klug G. A single flavoprotein, AppA, integrates both redox and light signals in *Rhodobacter sphaeroides*. Molecular Microbiology. 2002; 45:827–836. [PubMed: 12139627]
6. Han YC, Meyer MHF, Keusgen M, Klug G. A haem cofactor is required for redox and light signalling by the AppA protein of *Rhodobacter sphaeroides*. Molecular Microbiology. 2007; 64:1090–1104. [PubMed: 17501930]
7. Moskvin OV, Kaplan S, Gilles-Gonzalez MA, Gomelsky M. Novel heme-based oxygen sensor with a revealing evolutionary history. Journal of Biological Chemistry. 2007; 282:28740–28748. [PubMed: 17660296]
8. Gomelsky M, Klug G. BLUF: a novel FAD-binding domain involved in sensory transduction in microorganisms. Trends in Biochemical Sciences. 2002; 27:497–500. [PubMed: 12368079]
9. Gomelsky M, et al. Domain structure, oligomeric state, and mutational analysis of PpsR, the *Rhodobacter sphaeroides* repressor of photosystem gene expression. Journal of Bacteriology. 2000; 182:2253–2261. [PubMed: 10735869]
10. Elsen S, Jaubert M, Pignol D, Giraud E. PpsR: a multifaceted regulator of photosynthesis gene expression in purple bacteria. Molecular Microbiology. 2005; 57:17–26. [PubMed: 15948946]
11. Yamazaki Y, Fukusumi H, Kamikubo H, Kataoka M. Role of the N-terminal region in the function of the photosynthetic bacterium transcription regulator PpsR. Photochemistry and Photobiology. 2008; 84:839–844. [PubMed: 18282179]
12. Moskvin OV, Gomelsky L, Gomelsky M. Transcriptome analysis of the *Rhodobacter sphaeroides* PpsR regulon: PpsR as a master regulator of photosystem development. Journal of Bacteriology. 2005; 187:2148–2156. [PubMed: 15743963]
13. Cheng Z, et al. Activity of the tetrapyrrole regulator CrtJ is controlled by oxidation of a redox active cysteine located in the DNA binding domain. Molecular Microbiology. 2012; 85:734–46. [PubMed: 22715852]
14. Yin L, Dragnea V, Bauer CE. PpsR, a Regulator of Heme and Bacteriochlorophyll Biosynthesis, Is a Heme-sensing Protein. Journal of Biological Chemistry. 2012; 287:13850–13858. [PubMed: 22378778]
15. Anderson S, et al. Structure of a novel photoreceptor, the BLUF domain of AppA from *Rhodobacter sphaeroides*. Biochemistry. 2005; 44:7998–8005. [PubMed: 15924418]
16. Jung A, Reinstein J, Domratcheva T, Shoeman RL, Schlichting I. Crystal structures of the AppA BLUF domain photoreceptor provide insights into blue light-mediated signal transduction. Journal of Molecular Biology. 2006; 362:717–732. [PubMed: 16949615]
17. Grinstead JS, et al. The solution structure of the AppA BLUF domain: Insight into the mechanism of light-induced signaling. Chembiochem. 2006; 7:187–193. [PubMed: 16323221]
18. Jung A, et al. Structure of a bacterial BLUF photoreceptor: Insights into blue light-mediated signal transduction. Proceedings of the National Academy of Sciences of the United States of America. 2005; 102:12350–12355. [PubMed: 16107542]
19. Grinstead JS, Avila-Perez M, Hellingwerf KJ, Boelens R, Kaptein R. Light-induced flipping of a conserved glutamine sidechain and its orientation in the AppA BLUF domain. Journal of the American Chemical Society. 2006; 128:15066–15067. [PubMed: 17117839]

20. Konermann L, Pan J, Liu YH. Hydrogen exchange mass spectrometry for studying protein structure and dynamics. Chem Soc Rev. 2011; 40:1224–34. [PubMed: 21173980]
21. Jaubert M, et al. Light and redox control of photosynthesis gene expression in *Bradyrhizobium* - Dual roles of two PpsR. Journal of Biological Chemistry. 2004; 279:44407–44416. [PubMed: 15304477]
22. Whitty A. Cooperativity and biological complexity. Nat Chem Biol. 2008; 4:435–9. [PubMed: 18641616]
23. Bruscella P, Eraso JM, Roh JH, Kaplan S. The use of chromatin immunoprecipitation to define PpsR binding activity in *Rhodobacter sphaeroides* 2.4.1. Journal of Bacteriology. 2008; 190:6817–6828. [PubMed: 18689484]
24. Eraso JM, et al. Role of the global transcriptional regulator PrrA in *Rhodobacter sphaeroides* 2.4.1: Combined transcriptome and proteome analysis. Journal of Bacteriology. 2008; 190:4831–4848. [PubMed: 18487335]
25. Happ HN, Braatsch S, Broschek V, Osterloh L, Klug G. Light-dependent regulation of photosynthesis genes in *Rhodobacter sphaeroides* 2.4.1 is coordinately controlled by photosynthetic electron transport via the PrrBA two-component system and the photoreceptor AppA. Molecular Microbiology. 2005; 58:903–914. [PubMed: 16238636]
26. Dragnea V, Arunkumar AI, Yuan H, Giedroc DP, Bauer CE. Spectroscopic Studies of the AppA BLUF Domain from *Rhodobacter sphaeroides*: Addressing Movement of Tryptophan 104 in the Signaling State. Biochemistry. 2009; 48:9969–9979. [PubMed: 19746968]
27. Zoltowski BD, Gardner KH. Tripping the Light Fantastic: Blue-Light Photoreceptors as Examples of Environmentally Modulated Protein-Protein Interactions. Biochemistry. 2011; 50:4–16. [PubMed: 21141905]
28. Domratcheva T, Grigorenko BL, Schlichting I, Nemukhin AV. Molecular models predict light-induced glutamine tautomerization in BLUF photoreceptors. Biophysical Journal. 2008; 94:3872–3879. [PubMed: 18263659]
29. Han YC, Braatsch S, Osterloh L, Klug G. A eukaryotic BLUF domain mediates light-dependent gene expression in the purple bacterium *Rhodobacter sphaeroides* 2.4.1. Proceedings of the National Academy of Sciences of the United States of America. 2004; 101:12306–12311. [PubMed: 15292515]
30. Barends TRM, et al. Structure and mechanism of a bacterial light-regulated cyclic nucleotide phosphodiesterase. Nature. 2009; 459:1015–U150. [PubMed: 19536266]
31. Yuan H, Bauer CE. PixE promotes dark oligomerization of the BLUF photoreceptor PixD. Proceedings of the National Academy of Sciences of the United States of America. 2008; 105:11715–11719. [PubMed: 18695243]
32. Yuan H, Dragnea V, Wu Q, Gardner KH, Bauer CE. Mutational and structural studies of the PixD BLUF output signal that affects light-regulated interactions with PixE. Biochemistry. 2011; 50:6365–75. [PubMed: 21688827]
33. Fenno L, Yizhar O, Deisseroth K. The development and application of optogenetics. Annu Rev Neurosci. 2011; 34:389–412. [PubMed: 21692661]
34. Braatsch S, Moskvin OV, Klug G, Gomelsky M. Responses of the *Rhodobacter sphaeroides* transcriptome to blue light under semiaerobic conditions. Journal of Bacteriology. 2004; 186:7726–7735. [PubMed: 15516587]

Methods references

35. Van Duyne GD, Standaert RF, Karplus PA, Schreiber SL, Clardy J. Atomic structures of the human immunophilin FKBP-12 complexes with FK506 and rapamycin. J Mol Biol. 1993; 229:105–24. [PubMed: 7678431]
36. Kabsch W. XDS. Acta Crystallogr D Biol Crystallogr. 2010; 66:125–32. [PubMed: 20124692]
37. Adams PD, et al. PHENIX: a comprehensive Python-based system for macromolecular structure solution. Acta Crystallogr D Biol Crystallogr. 2010; 66:213–21. [PubMed: 20124702]
38. Emsley P, Lohkamp B, Scott WG, Cowtan K. Features and development of Coot. Acta Crystallogr D Biol Crystallogr. 2010; 66:486–501. [PubMed: 20383002]

Europe PMC Funders Author Manuscripts

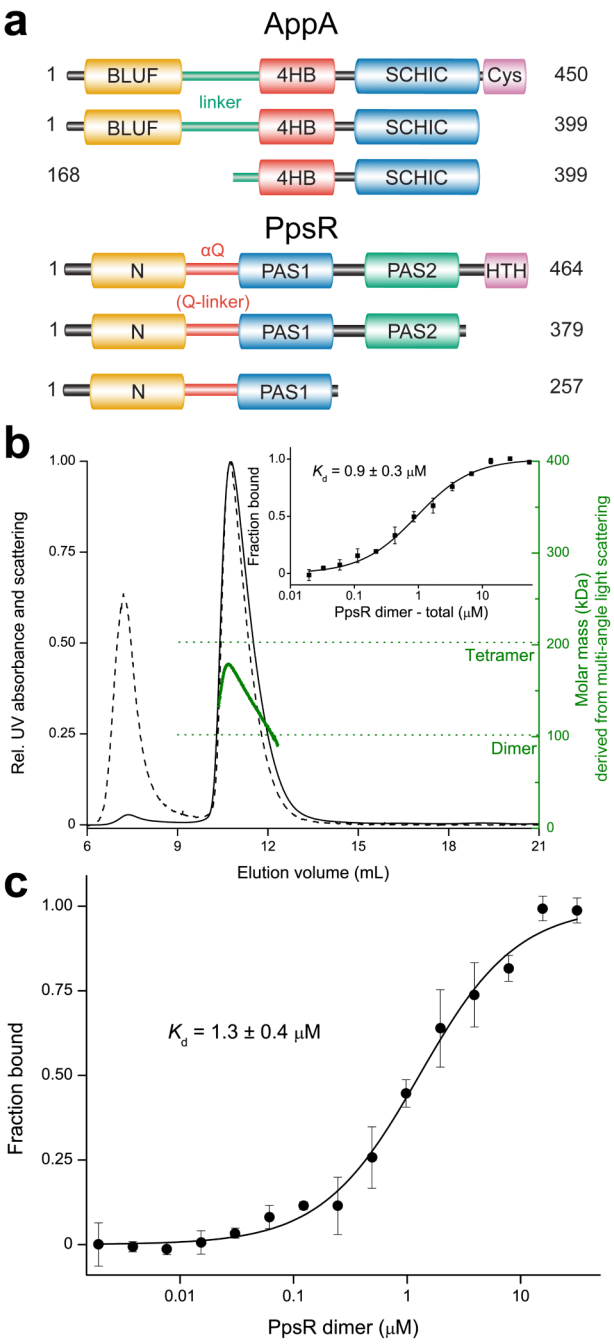

Figure 1. AppA and PpsR domains involved in AppA–PpsR$_2$ formation and PpsR tetramerization

(**a**) The upper part shows protein constructs of AppA used in this study color-coded according to domains described previously or identified in the crystal structure presented here: BLUF – orange; linker region including the BLUF capping helix – bluish green; 4HB – red; SCHIC – blue and cysteine-rich – purple. The lower part depicts PpsR constructs of this study colored according to: N-domain – orange; αQ – red; PAS1 – blue; PAS2 – bluish green and HTH – purple. (**b**) Normalized MALS detection of PpsR fractionated by size exclusion chromatography (solid – UV absorbance, dashed – scattering signal). The calculated molar mass signal is plotted in green. The inset shows the quantification of the

oligomer equilibrium using MST resulting in a K_d of 0.9 μM based on dimer concentration. Error bars represent the standard deviation of three individual experiments. (**c**) Quantification of the $AppA_{\Delta C}$–$PpsR_2$ interaction using MST resulted in a K_d of 1.3 μM calculated for a PpsR dimer as binding partner. MST measurements were performed at 25 °C in triplicate and error bars correspond to the standard deviation.

Europe PMC Funders Author Manuscripts

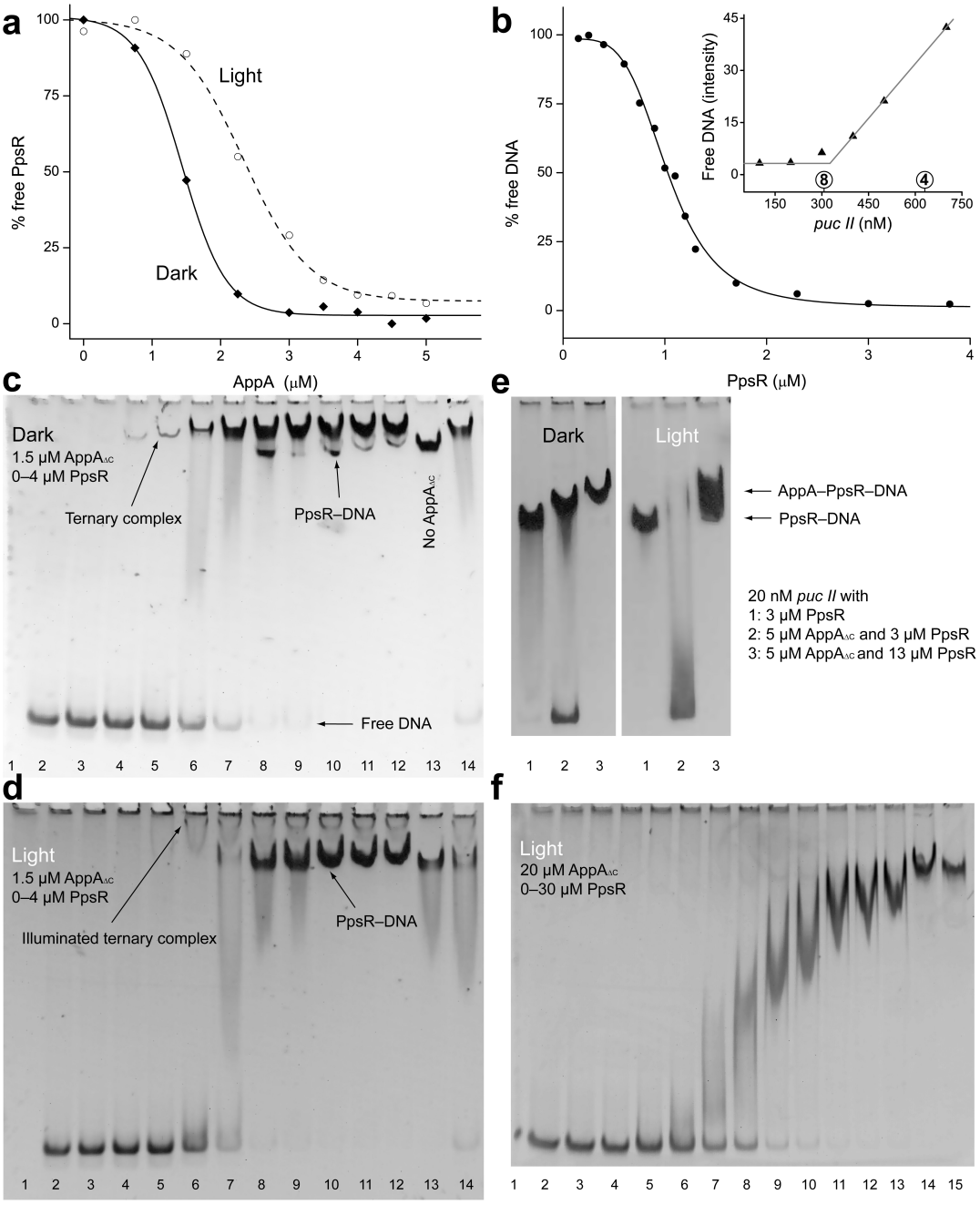

Figure 2. $AppA_{\Delta C}$–$PpsR_2$ formation allows light-control of PpsR-binding to DNA

(**a**) Quantification of native PAGE experiments addressing $AppA_{\Delta C}$–$PpsR_2$ formation under dark (solid) and light (dashed) conditions. PpsR (3 μM) was titrated with $AppA_{\Delta C}$ (Supplementary Fig. 2**b**,**c**) (**b**) DNA-binding curve of PpsR obtained from two complementary titrations of *puc I* (Supplementary Fig. 3**a**). The inset shows an active site titration of PpsR (2.5 μM) with *puc II*. The circled 4 and 8 reflect theoretical transition points for tetramer or octamer binding, respectively. (**c**) EMSA showing $AppA_{\Delta C}$–$PpsR_2$–DNA complex formation upon PpsR titration of *puc I* with 1.5 μM $AppA_{\Delta C}$ present. Lanes 2–12 – PpsR concentrations from 0 to 4 μM (details in Supplementary Fig. 3**d**), lane 13 – 2

Europe PMC Funders Author Manuscripts

μM PpsR without $AppA_{\Delta C}$ and lane 14 – 2 μM PpsR with dark-recovered $AppA_{\Delta C}$. (**d**) Analogous EMSA to panel **c** with illumination. The ternary complex is shifted towards the well (Coomassie stain in Supplementary Fig. 3**e**). (**e**) EMSAs under dark- and light-conditions using *puc II* and $AppA_{\Delta C}$ concentrations enabling saturation of $AppA_{\Delta C}$–$PpsR_2$. Lane 1 – 3 μM PpsR, lane 2 – 5 μM $AppA_{\Delta C}$ + 3 μM PpsR and lane 3 – 5 μM $AppA_{\Delta C}$ + 13 μM PpsR (protein stains in Supplementary Figure 3**f**). (**f**) Illuminated EMSA addressing light-stability of the ternary complex with *puc II* in the presence of 20 μM $AppA_{\Delta C}$ enabling saturation of $AppA_{\Delta C}$–$PpsR_2$ throughout the PpsR titration. Lanes 1–15 – 0, 0.1, 0.25, 0.5, 1, 1.5, 2.5, 3.5, 4.5, 5.5, 6.5, 7.5, 10, 20, 30 μM PpsR.

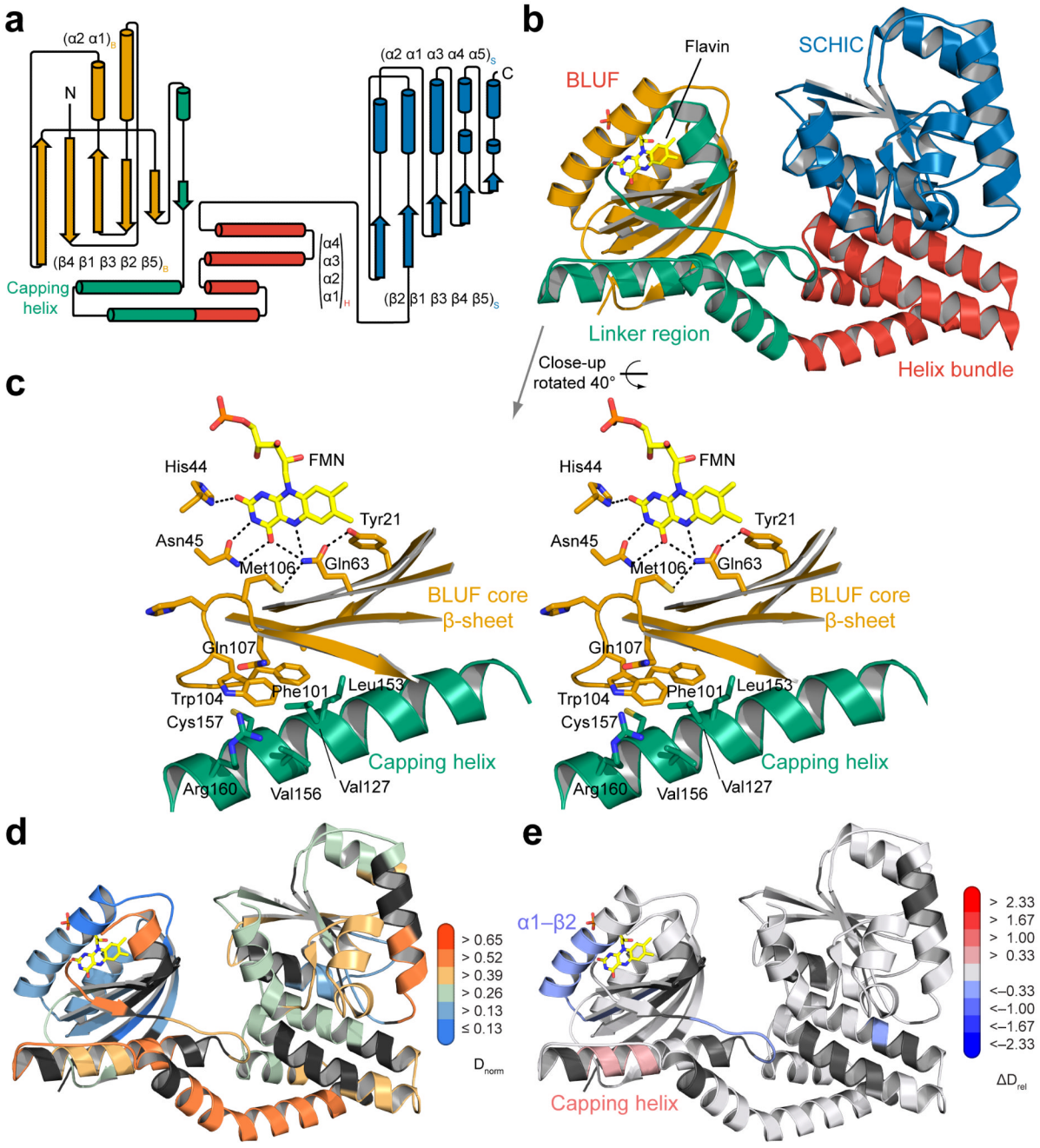

Figure 3. Domain organization of AppA supports the dual sensor function

(**a**) Secondary structure representation of AppA with individual domains color-coded according to Fig 1**a**. (**b**) Overall $AppA_{\Delta C}$ structure with domains colored according to panel **a**. (**c**) Stereo-view of conserved BLUF residues around the flavin cofactor (yellow) showing the positioning of Trp104. Residues contacting Trp104 from the core β-sheet and the capping helix are shown as stick models. (**d**) $AppA_{\Delta C}$ structure colored with respect to deuterium incorporation in the dark after 15 s labeling. Implications of the color-coding and details for the normalization procedure (D_{norm}) are described in the Supplementary Note. (**e**)

Changes in relative deuterium incorporation between dark and blue-light conditions after 15 s labeling. Details of the color-coding are described in the main text.

Europe PMC Funders Author Manuscripts

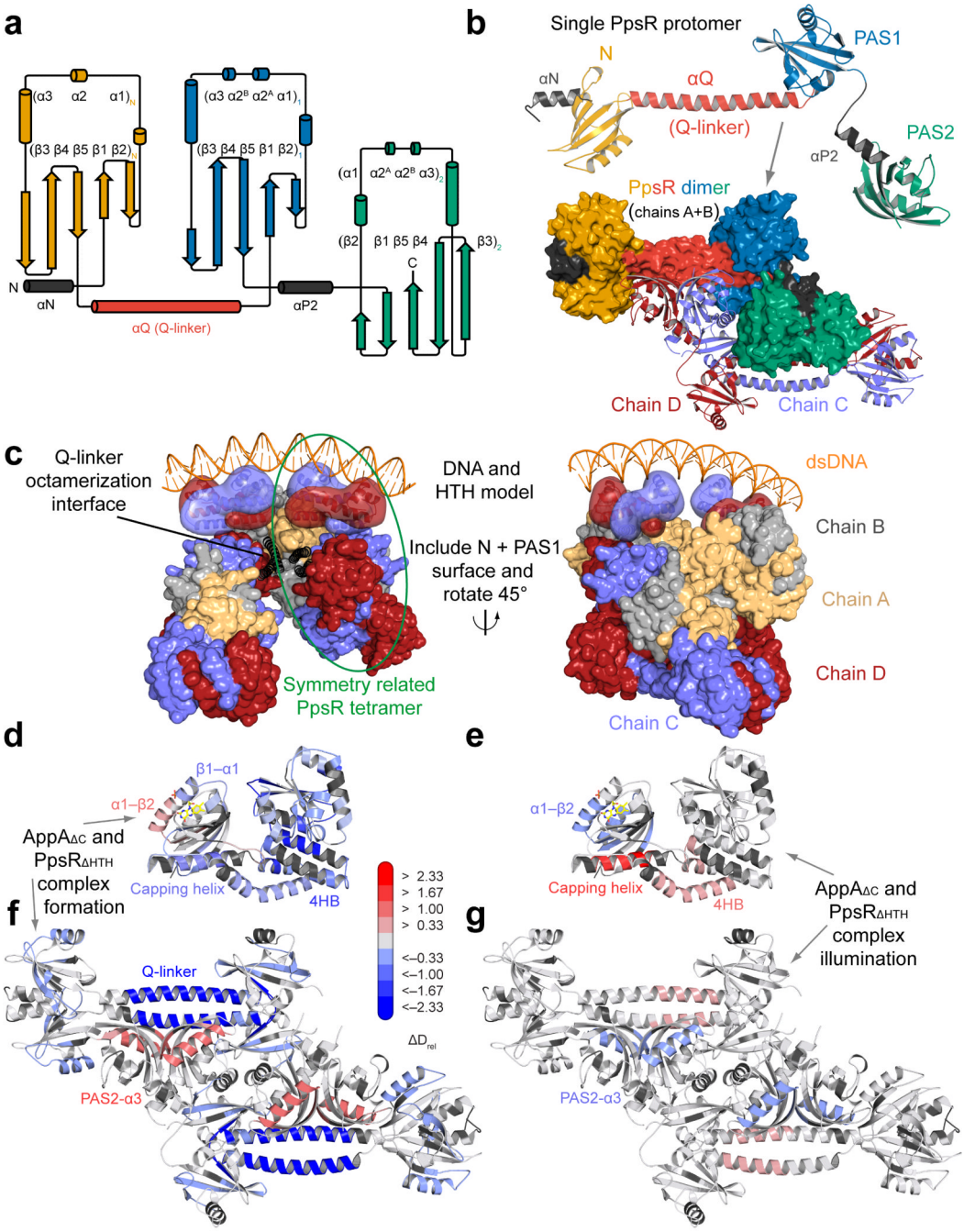

Figure 4. Structural characterization of PpsR with implications for DNA-binding and AppA$_{\Delta C}$–PpsR$_2$ complex formation

(**a**) Secondary structure representation of PpsR color-coded according to Fig 1**a**. Helices αN and αP2 (grey) correspond to N-terminal helices of the N- and the PAS2-domains, respectively. (**b**) Domain architecture of a single PpsR$_{\Delta HTH}$ protomer colored according to panel **a**. Parallel dimerization is shown in the lower part in surface representation. An anti-parallel dimer colored in light-blue and dark-red according to individual protomers of chains C and D completes the tetrameric assembly. (**c**) Model for PpsR-binding to DNA based on the crystallographic octamer. The αQ (black helices) mediated interaction between symmetry-related tetramers enables close positioning of two HTH dimers. HTH models

Europe PMC Funders Author Manuscripts

(transparent surface) together with the DNA double helix are based on the Fis structure (pdb 3JRE). HTH dimers extend from the PAS2 C-termini and are rotated to account for DNA-binding and tilted to prevent clashes. Colors correspond to protomers (panel **b**) with light-orange and grey for chains A and B, respectively. (**d**,**e**) Changes in D_{rel} upon complex formation for $AppA_{\Delta C}$ and PpsR mapped on the structures of $AppA_{\Delta C}$ and $PpsR_{\Delta HTH}$, respectively. (**f**,**g**) Changes in D_{rel} upon illumination of $AppA_{\Delta C}$–$PpsR_2$ mapped on both structures. The 15 s time points are shown in panels **d**, **e** and **g** for visualization of regions protected through complexation (blue), whereas the 60 s time point in panel **f** was chosen to additionally demonstrate the increased exchange dynamics (red) of a 4HB peptide.

Europe PMC Funders Author Manuscripts

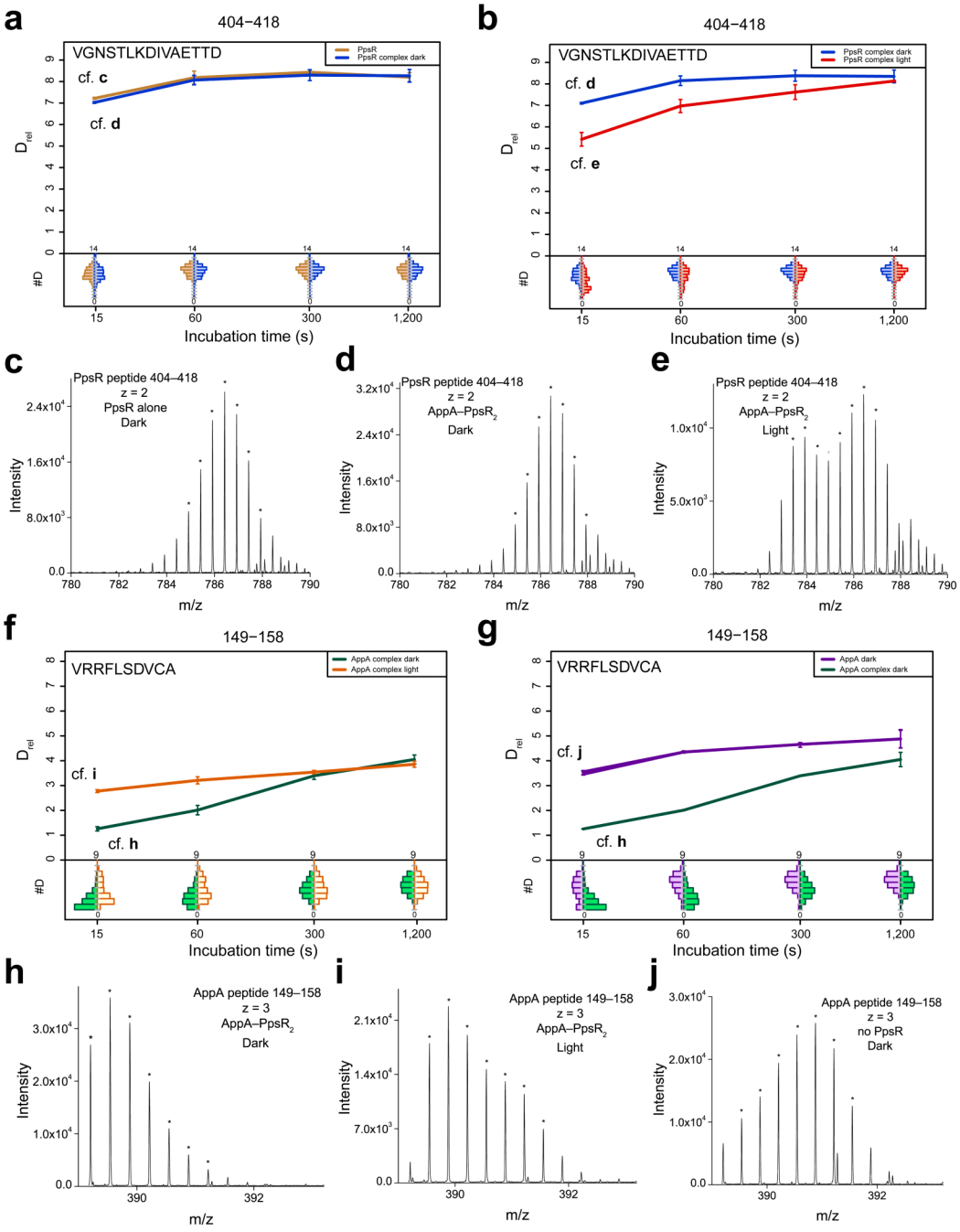

Figure 5. HDX details of PpsR-HTH and the AppA-BLUF capping-helix

(**a**,**b**) Deuterium uptake plots of a HTH-peptide in free PpsR (brown) and after complex formation with dark-state $AppA_{\Delta C}$ (blue, panel **a**), as well as for $AppA_{\Delta C}$–$PpsR_2$ under light-conditions (red, panel **b**). Main sub-panels show D_{rel} plotted against labeling time for the peptide specified at the top. The estimated abundance distribution of individual deuterated species is presented in the lower sub-panels on a scale from undeuterated to all exchangeable amides deuterated. The observation of a bimodal distribution points to the presence of an $AppA_{\Delta C}$–$PpsR_2$ species with the HTH motif in a conformation different to dark-adapted complex or free PpsR. (**c**,**d**,**e**) To assess the quality of evaluated data selected

raw-spectra are shown for the 15 s time points of one HTH-peptide of free PpsR, dark-adapted $AppA_{\Delta C}$–$PpsR_2$ and light-state $AppA_{\Delta C}$–$PpsR_2$, respectively. The seven most intense isotope peaks of the series of interest are marked with an asterisk. (**f**,**g**) Comparison of deuterium uptake of an AppA-BLUF capping-helix peptide between $AppA_{\Delta C}$–$PpsR_2$ under dark- (green) and light-conditions (orange, panel **f**), as well as in free AppA (purple, panel **g**). Note the broad distribution of deuterated species in free AppA indicating again EX1-like exchange kinetics. Complex formation shifts the equilibrium of the two conformations responsible for bimodal deuteration to one state, which can be partially reverted by illumination. (**h**,**i**,**j**) Raw data of 15 s time points of dark-adapted $AppA_{\Delta C}$–$PpsR_2$, light-state $AppA_{\Delta C}$–$PpsR_2$ and free AppA, respectively.

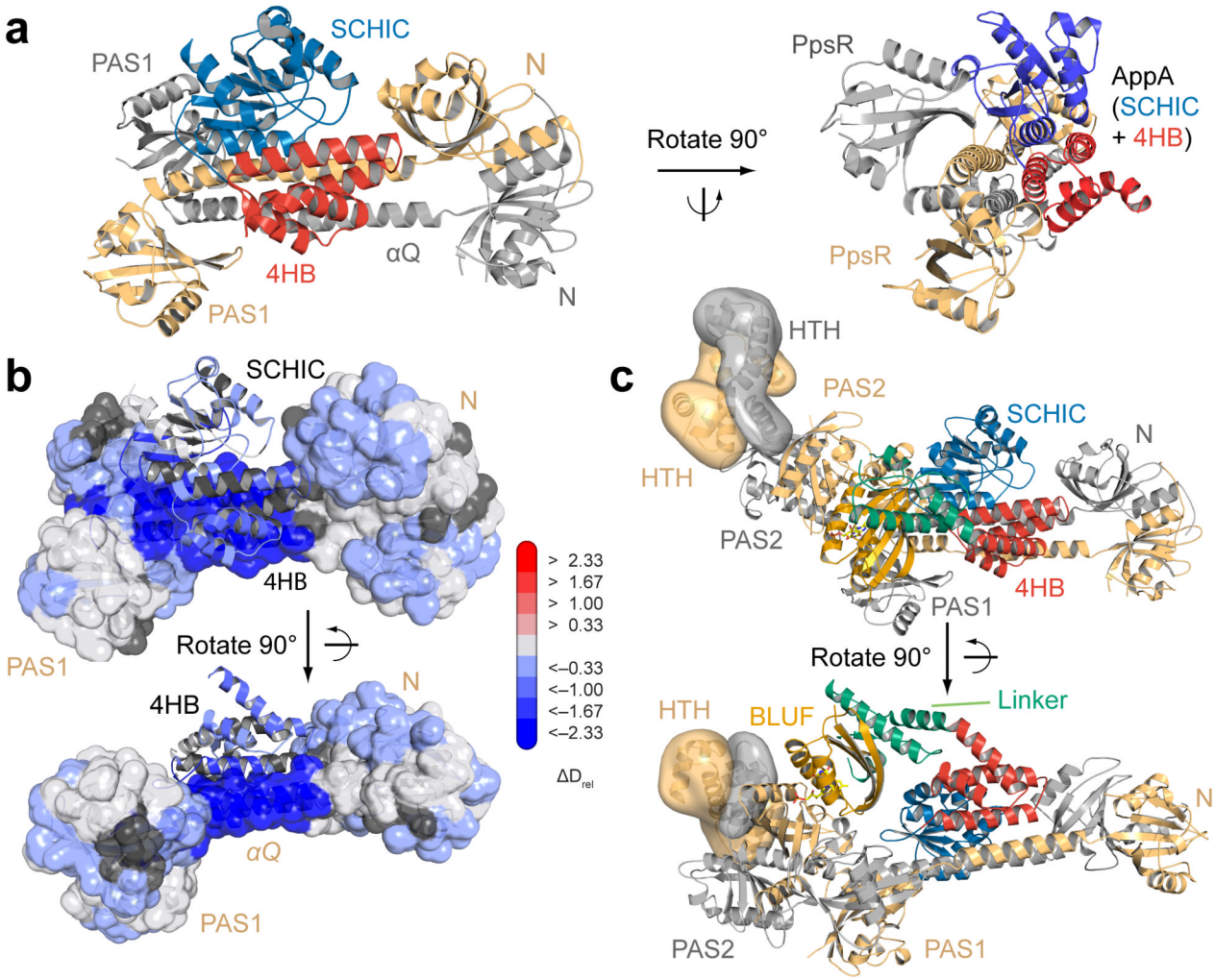

Figure 6. Molecular details of the AppA–PpsR$_2$ core interface

(**a**) Overall structure of the core complex color-coded according to domains of AppA (Fig. 3**b**) and protomers A and B of PpsR (Fig. 4**c**). Details of the interface are described in the text. (**b**) Superposition of HDX data with the observed complex interface. Data of the 15 s time points, as shown in Figure 4**d** and **f**, are mapped on the core complex with N–Q–PAS1 shown in transparent surface and the AppA domains in cartoon representation. The full time course can be seen in Supplementary Movie 6. (**c**) The model of the AppA$_{\Delta C}$–PpsR$_2$ complex is based on the individual structures after aligning the PAS1 dimers of PpsR$_{\Delta HTH}$ and 4HB and SCHIC of AppA$_{\Delta C}$, respectively. The HTH domains are placed in analogy to Figure 4**c**.

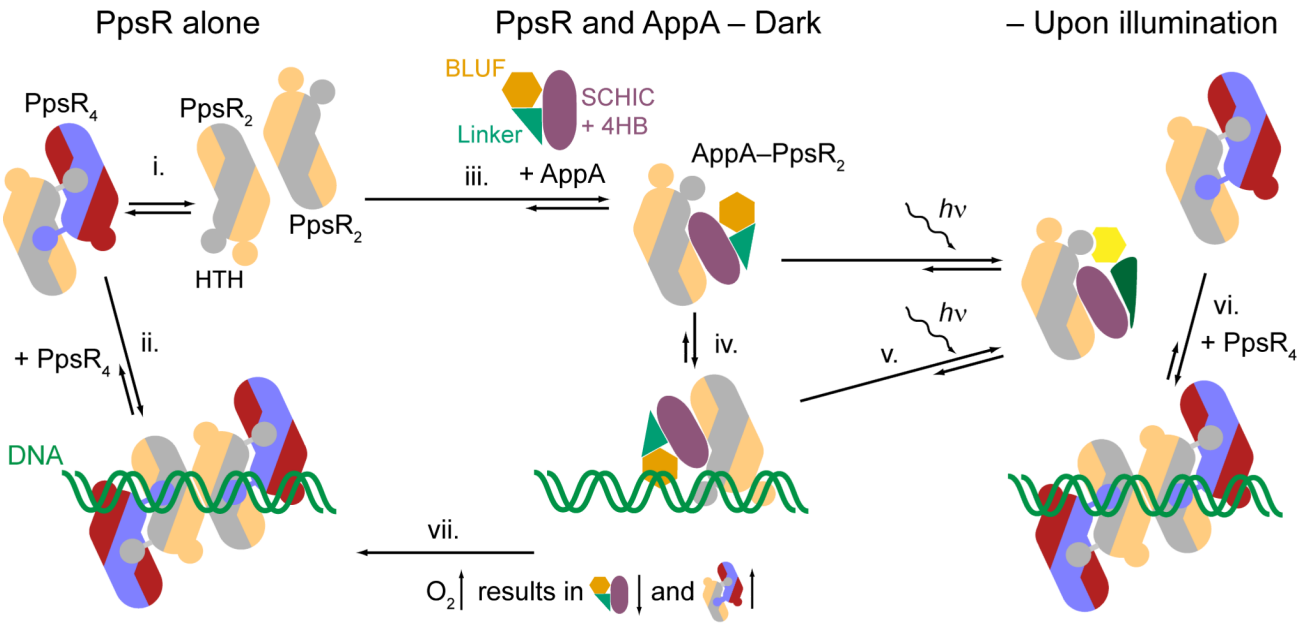

Figure 7. A new model for controlling photosynthetic gene expression by AppA and PpsR in a light- and oxygen-dependent manner

(**i.**) PpsR exists in a dimer-tetramer equilibrium and (**ii.**) binds to promoter regions of regulated genes as an octamer (colored according to Fig. 4**c**). (**iii**.) Addition of AppA leads to the formation of AppA–$PpsR_2$. (**iv.**) This species also interacts with the promoter region forming a ternary protein-DNA complex. (**v.**) Illumination of this complex does not lead to dissociation of AppA and PpsR but reduces the affinity for DNA. Depending on the relative concentrations of AppA and PpsR, (**vi**.) excess PpsR competes successfully with AppA–$PpsR_2$ for promoter regions under light conditions but is not able to replace the ternary complex in the dark. (**vii.**) The levels of AppA and PpsR are inversely regulated in response to oxygen availability. An increase in oxygen concentration favors the formation of the $PpsR_8$–DNA species leading to enhanced repression of photosynthesis gene transcription. The model depicted accomodates *in vivo* results presented for anaerobic[3,25], semi-aerobic[4,5,34] and higher oxygen conditions[3,23,24].

Europe PMC Funders Author Manuscripts

Table 1

Data collection, phasing and refinement statistics (combined Se-SAD and molecular replacement)

	AppA Δ399 C20S Se-SAD[§]	AppA Δ399 C20S	AppA Δ399 wild-type	PpsR ΔHTH Se-SAD[§]	PpsR ΔHTH	AppA–PpsR2 core complex
Data collection						
Space group	$P3_212$	$P3_212$	$P3_212$	$P3_221$	$P3_221$	$P2_12_12$
Cell dimensions						
a, *b*, *c* (Å)	70.5, 70.5, 381.5	70.3, 70.3, 382.1	70.5, 70.5, 383.8	117.8, 117.8, 211.0	117.5, 117.5, 211.8	89.8, 188.3, 51.9
α, *β*, *γ* (°)	90.0, 90.0, 120.0	90.0, 90.0, 120.0	90.0, 90.0, 120.0	90.0, 90.0, 120.0	90.0, 90.0, 120.0	90.0, 90.0, 90.0
	Peak			*Peak*		
Wavelength	0.9786	1.0000	1.0000	0.9790	0.9483	0.9998
Resolution (Å)	50 - 3.9 (4.0 - 3.9)*	48 - 2.6 (2.7 - 2.6)	58 - 3.5 (3.6 - 3.5)	60 – 5.5 (5.6 – 5.5)	50 – 2.8 (2.9-2.8)	50 - 1.75 (1.85 - 1.75)
R_{merge}	0.084 (0.177)	0.052 (0.629)	0.154 (0.836)	0.094 (0.340)	0.043 (0.681)	0.053 (0.684)
$I / \sigma I$	33.6 (20.2)	18.2 (2.63)	9.90 (2.45)	30.9 (12.2)	17.4 (2.7)	20.3 (2.85)
Completeness (%)	99.7 (99.3)	99.7 (99.8)	99.6 (99.9)	99.9 (100)	99.0 (99.6)	99.9 (99.9)
Redundancy	20.0 (20.1)	5.5 (5.7)	4.4 (4.6)	21.8 (22.9)	5.2 (5.2)	8.6 (8.5)
Refinement						
Resolution (Å)	-	47.6 - 2.6	58.2 - 3.5	-	47.0 - 2.8	44.9 - 1.75
No. reflections	-	33,844	14,209	-	41,952	89,590
R_{work} / R_{free}	-	0.1849 / 0.2267	0.1860 / 0.2257	-	0.1815 / 0.2348	0.1699 / 0.1980
No. atoms	-	5960	5862	-	11495	6221
Protein	-	5800	5800	-	11484	5538
Ligand/ion	-	62/18	62	-	-	-
Water	-	80	-	-	11	683
B factors	-	76.8	80.7	-	85.3	31.3
Protein	-	76.9	80.4	-	85.3	30.5
Ligand/ion	-	83.7	109	-	-	-
Water	-	63.2	-	-	59.6	37.7
r.m.s. deviations						
Bond lengths (Å)	-	0.005	0.008	-	0.005	0.006
Bond angles (°)	-	0.87	1.04	-	0.84	1.02

[§] Statistics reported to the cut-off used for anomalous data processing.

* Values in parentheses are for highest-resolution shell.